J. Korean Inst. Electr. Electron. Mater. Eng.
Vol. 36, No. 5, pp. 423-432 September 2023
doi: https://doi.org/10.4313/JKEM.2023.36.5.1
ISSN 1226-7945(Print), 2288-3258(Online)

Academic Progress Report

최근 터치스크린 Readout 시스템의 연구 경향

이준민, 함주원, 장우석, 이하민, 구상모, 오종민, 고승훈
광운대학교 전자재료공학과

Recent Research Trends in Touchscreen Readout Systems

Jun-Min Lee, Ju-Won Ham, Woo-Seok Jang, Ha-Min Lee, Sang-Mo Koo, Jong-Min Oh, and Seung-Hoon Ko
Department of Electronic Materials Engineering, Kwangwoon University, Seoul 01897, Korea

(Received July 5, 2023; Revised August 7, 2023; Accepted August 8, 2023)

Abstract: With the increasing demand for mobile devices featuring multi-touch operation, extensive research is being conducted on touch screen panel (TSP) Readout ICs (ROICs) that should possess low power consumption, compact chip size, and immunity to external noise. Therefore, this paper discusses capacitive touch sensors and their readout circuits, and it introduces research trends in various circuit designs that are robust against external noise sources. The recent state-of-the-art TSP ROICs have primarily focused on minimizing the impact of parasitic capacitance (Cp) caused by thin panel thickness. The large Cp can be effectively compensated using an area-efficient current compensator and Current Conveyor (CC), while a display noise reduction scheme utilizing a noise-antenna (NA) electrode significantly improves the signal-to-noise ratio (SNR). Based on these achievements, it is expected that future TSP ROICs will be capable of stable operation with thinner and flexible Touch Screen Panels (TSPs).

Keywords: Touch sensor, Readout integrated circuit, Noise antenna, Signal to noise ratio

1. INTRODUCTION

The growth of the Internet-of-Things (IoT) market has been recently fueled by advancements in artificial intelligence and wearable device technologies. These technologies have been successfully developed across diverse sectors including entertainment, fitness, gaming, and healthcare. Thus, the wearable devices market was estimated to be around USD 80 billion in 2020 and is projected to reach USD 138 billion by 2025 [1]. Due to constraints on battery capacity, the operating systems in wearable devices demand both a compact chip area and minimal power consumption. Consequently, the miniaturization and power-efficiency of these devices have become significant factors of competitiveness. In the field of display panels, producing a capacitive TSP display panel is one of the significant challenges. Such a panel encompasses transparent TSP electrodes, liquid crystal (LC) or organic light-emitting diode (OLED) display pixels, a display driver IC, and a TSP readout IC (ROIC). Correspondingly, many state-of-the-art capacitive TSP ROICs have been developed to enhance the signal-to-noise ratio (SNR) and scan rate while simultaneously reducing power consumption.

Capacitive TSP readout systems are classified into self-capacitive and mutual-capacitive sensing techniques. Mutual-capacitive sensing TSP consists of several transmitting (Tx) and receiving (Rx) electrodes, with mutual-capacitance arising

✉ Jong-Min Oh; jmoh@kw.ac.kr
Seung-Hoon Ko; shko@kw.ac.kr

at each Tx-Rx intersection. In contrast, in self-capacitance measurement, both driving and sensing are applied to a single TSP electrode. In both readout systems, external noises coupled via the TSP's parasitic capacitances can degrade the SNR. Otherwise, the sensitivity can be enhanced at the expense of decreased scan rate and increased power consumption.

In TSP readout systems, it's typically necessary to have a touch scan rate of 120 Hz, which is equal to the display refresh rate of recent smartphone. If the touch scan rate falls below the display refresh rate, users may experience noticeable touch latency. To achieve the necessary scan rate, TSP ROICs often utilize TSP driving signals with a frequency higher than the panel's bandwidth. In this case, it may result in issues related to sensitivity deviation among the TSP nodes.

Touch spatial resolution can also be affected by several trade-offs, including response time, power consumption, the pitch of TSP channels, and the optimization of algorithms. For example, in a display panel with a large pitch of TSP channels, a spatial filter that weights previous frame touch data is necessary. However, this leads to an increased moving latency with finger movement. Otherwise, to minimize the jitter when a finger remains stationary on a panel with large TSP channel pitch, scan time should be increased. While this can improve the SNR, it also results in higher power consumption of the ROIC.

In this paper, we briefly review the state-of-the-art TSP readout systems. Section 2 details the system architecture and operational principles of capacitive TSP readout systems. In Section 3, the design considerations for minimizing noise interference are described, and Section 4 briefly introduces the research trends in ROIC designs. Finally, a conclusion is offered in Section 5.

2. CAPACITIVE SENSOR AND READOUT CIRCUIT

In this section, the fundamentals of a typical capacitive touch readout system are introduced. As depicted in Fig. 1, the TSP readout system primarily consists of a TSP sensor, an analog front-end (AFE) for measuring changes in self- and mutual-capacitances, an analog-to-digital converter (ADC) for converting the sensed signals into digital codes, and a microcontroller unit (MCU). The MCU is responsible for conducting baseline calibration, coordinate interpolation, and software filtering to precisely determine the point of touch.

2.1 Capacitive sensor

A capacitor consists of two conductive electrodes, with a dielectric material between them. The capacitance value is determined by the distance between the electrodes, the physical area of the electrodes, and the permittivity ($C = \varepsilon A/d$). Using these properties of a capacitor, a capacitive sensing system can detect changes in capacitance when a conductor such as a finger comes into contact.

Capacitive sensors are employed in a wide range of modern applications as shown in Fig. 2. They offer significant advantages over other types of sensors, such as resistive or infrared radiated proximity sensors. First, their high sensitivity enables the precise detection of minute changes in capacitance, making them suitable for proximity detection and displacement sensing tasks [2]. Therefore, a key advantage is its capability to perform non-contact sensing of an object, an essential feature for dealing with delicate or easily disturbed targets. Furthermore, the capacitive sensors can operate robustly and reliably in diverse environmental conditions, including those with dust and variable light sources, and fluctuating temperatures. They also have the versatility to detect both metallic and non-metallic targets, including

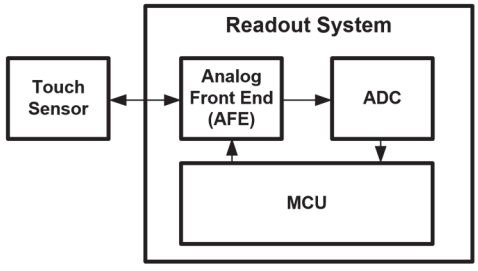

Fig. 1. Block diagram of TSP readout system.

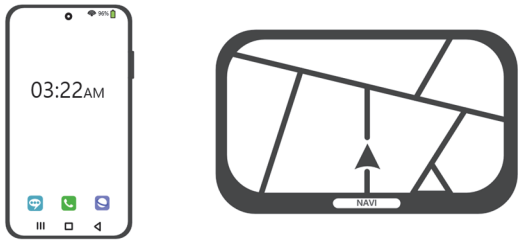

Fig. 2. Applications of capacitive sensing system.

various types of materials such as solids, liquids, and gases. Lastly, the manufacturing simplicity and durability of capacitive sensors contribute to their cost-effectiveness, making them an economical choice for a variety of applications.

2.1.1 Self-capacitive sensor

Capacitive TSP sensing schemes can be classified into two categories: self-capacitance (C_S) and mutual-capacitance (C_M) sensing methods. Especially, the C_S-sensing is a primary technology employed in many touchscreen applications. Figure 3(a) illustrates the operation principle of a conventional C_S-sensing scheme for touch readout systems. This method detects changes in electrical capacitance as a user's hand or finger approaches the TSP sensor, thereby determining the location of touch points. The voltage pulses are applied to the TSP electrodes while the returned voltages or currents are measured to sense changes in C_S. The presence of a user's finger disturbs the electric field due to the finger's conductivity. This disruption is perceived as a change in capacitance between the TSP electrodes and ground, which is subsequently detected by the readout system and interpreted as a touch. As a result, the base capacitance, which was the C_{S1} (and C_{S2}), increases by finger capacitance ΔC_{S1} (and ΔC_{S2}). A key advantage of C_S-sensing is its high sensitivity and precision, providing a clear touch response. Even a minor change in the electric field from proximity of fingers [2-5] can cause a measurable change in capacitance, enabling 3-dimensional (D) hover gesture recognition, as shown in Fig. 3(b). The capability of these sensors to detect such minute changes is owing to its high sensitivity. However, a notable limitation of this sensing method is its inherent difficulty with multi-touch scenarios. A potential solution to overcome this limitation is the application of C_M-sensing.

2.1.2 Mutual-capacitive sensor

Mutual-capacitance (C_M) sensing is a widely used sensing method in touchscreen technology. The overall working principle is similar to that of the C_S-sensing except that it detects capacitive changes between two TSP electrodes.

In the C_M-sensing, a grid of electrodes through which current flows is positioned over the screen, forming a small capacitor (C_M) at each intersection of the Tx and Rx electrodes, depicted in Fig. 4(a). When a user touches the screen, their conductive finger disrupts the electric field at the intersection, causing a change in the capacitance of the respective capacitor nodes.

As a result, the base capacitance of C_M decreases by the parallel capacitance of C_{M1} and C_{M2}. This change in capacitance is detected by the TSP ROIC and used to determine the location of the touch. The C_M-sensing is particularly beneficial for its precise detection of multi-touch scenarios. Since the capacitive changes at each capacitor are individually measured, the system is capable of identifying and tracking multiple

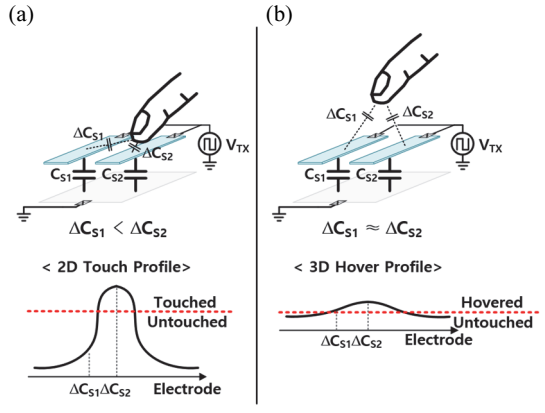

Fig. 3. Self-capacitive sensor for (a) typical 2-dimensional touch and (b) 3-dimensional proximity detection.

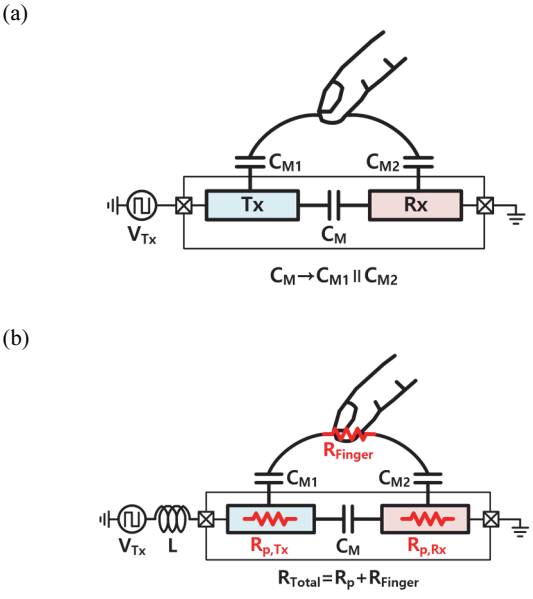

Fig. 4. Mutual-capacitive sensor in (a) typical 2D touch and (b) finger resistance detection system.

touch points concurrently.

Nevertheless, this technology can introduce higher complexity and costs. These come from the necessity for 2-layer sensor electrodes to form the capacitance nodes, perform measurements at each node intersection, and interpret these measurements. Another application of this technology enables the measurement of finger resistance (R_{Finger}) with mutual-capacitive sensing system [6], as illustrated in Fig. 4(b). The resonant frequency of the sensors is determined by the change in the mutual-capacitance and an externally connected inductor with inductance denoted as L. By transmitting a driving signal at the resonant frequency of $2\pi \times 1/[L(C_{M1} \| C_{M2})]^{1/2}$, the impedance consisting of a series combination of L, C_M, R_p, and R_{Finger} becomes only the impedance of resistances. Consequently, the output of readout system can be represented as a function of only R_{Finger}.

2.2 Analog front-end circuit

Based on the type of capacitances (C_S or C_M), the TSP readout circuit can be categorized into two types: self-capacitive sensing and mutual-capacitive sensing circuits. The capacitive change in C_S (or C_M) caused by a finger contact to the TSP is extracted and converted into a form of charge, current, or voltage. The subsequent ADC then converts these values into digital codes, which are utilized in coordinate calculations to find exact touch locations. In this section, several TSP AFE architectures are analyzed in detail, taking into account the types of TSP capacitances.

2.2.1 Self-capacitive readout circuit

Figures 5(a) and (b) shows the C_S-sensing circuit and its operational timing diagram. To sense C_S, the switched-capacitor integrator (SC-INT) circuit operates in two phases. During Φ_1=1 phase, the C_S is charged with supply voltage (=V_{DD}), and in the Φ_2=1 phase, the signal stored in the C_S is dis-charged to the feedback capacitor (C_{FB}). Because of the negative feedback of operational amplifier (op-amp), the (-) input of the op-amp is fixed to half of the supply voltage ($V_{DD}/2$), transferring the charge of $C_S \times V_{DD}/2$. The SC-INT circuit continually accumulates the transmitted charges on the C_{FB}, creating a moving average filtering effect (MAF). This relationship is represented in Equation (1).

(a)

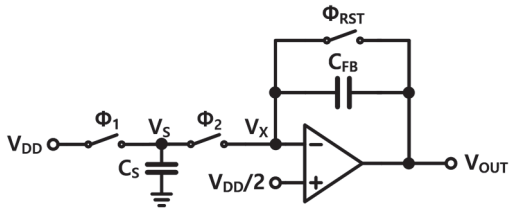

(b)

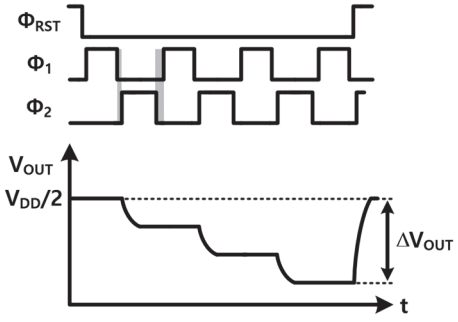

Fig. 5. (a) Self-capacitive sensing with charge integrator and (b) timing-diagram.

$$\frac{1}{2}V_{DD} \cdot \frac{C_S}{C_{FB}} = \Delta V_{acc} \tag{1}$$

$$3\Delta V_{acc} = \Delta V_{OUT} \tag{2}$$

The signal accumulated on the C_{FB} is finally converted to digital codes and reset for the next conversion phase. As will be discussed in section 4, the voltage nodes of subsequent sensing blocks can become saturated due to a large C_S, which normally occurs in flexible display panels. Hence, a separate C_S-compensation circuit is necessary to offset static C_S. Consequently, the accumulation of an additional charge equivalent to this change results in a significant variation in V_{OUT}.

2.2.2 Mutual-capacitive readout circuit

The operation of C_M-sensing circuit is depicted in Fig. 6. Similar to the C_S-sensing circuit [Fig. 5(a)], the mutual SC-INT circuit operates in two phases. During the high phase of Φ_1, the C_M is charged to $C_M \times V_{DD}$. Subsequently, when Φ_2 is high, the charges on C_M moves towards the left side of C_{FB}, increasing the V_{OUT}. The amount of transferred charge is described in Equation (3) and the corresponding relation is represented in Equation (4).

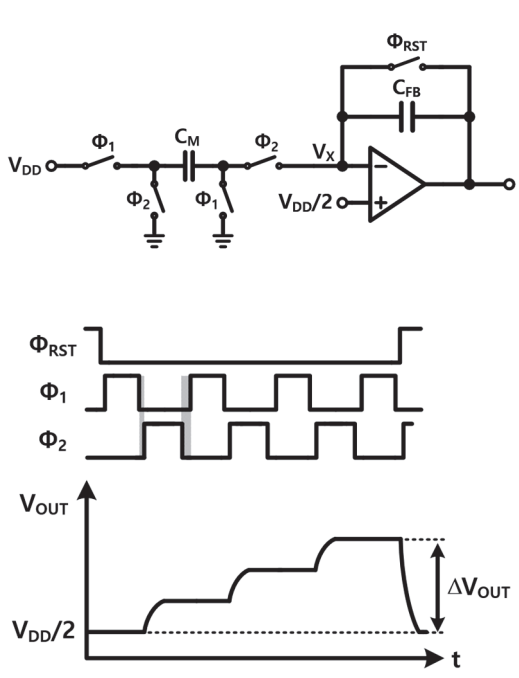

Fig. 6. (a) Mutual-capacitive sensing with charge integrator and (b) timing-diagram.

$$Q = \frac{1}{2} V_{DD} \cdot C_M = \Delta V_{OUT} \cdot C_{FB} \quad (3)$$

$$\frac{1}{2} V_{DD} \cdot \frac{C_M}{C_{FB}} = \Delta V_{acc} \quad (4)$$

Because the C_M-sensing circuit measures the fringing field between TSP's Tx and Rx electrodes as illustrated in Fig. 4(a), when a finger touches the TSP, it disrupts this field, resulting in a decrease in the C_M.

3. NOISE ISSUES

In commercial TSP products, the performance of the TSP ROIC largely depends on the ability to suppress various noise sources that interfere with the TSP. This section discusses the intrinsic and external noise sources in the TSP readout system, and describes established AFE architectures designed to minimize these noise sources. Thus, this can enhance the SNR and improve the overall performance of the TSP ROIC.

3.1 Intrinsic-circuit noise issues

The readout system itself usually generates intrinsic noise, primarily due to the many operational amplifiers (op-amps) in the ROIC. These op-amps often exhibit non-ideal characteristics like finite open-loop gain, limited slew rate, bandwidth, nonlinearity, offset, and flicker (1/f) noise. Among these, 1/f noise is a significant noise source for the ROIC, and it can be mitigated using a technique known as 'chopping' [7], which will be discussed in detail later. Moreover, the offset of the op-amp can be corrected using the Correlated Double Sampling (CDS) technique. Several other strategies exist [8-10] to enhance the performance of the op-amp. These approaches are all designed to improve the overall system performance by decreasing noise and enhancing signal integrity.

3.2 External noise issues

External noises coupled to the TSP can generally be categorized into three types: HUM noise, Display noise, and Switch Mode Power Supply (SMPS) noise. HUM noises are typically generated when mobile devices are powered by alternating current (AC), with a frequency range of 50 Hz and 60 Hz. Display noise, on the other hand, is injected when the display pixels are driven periodically, which are located beneath the TSP electrodes in the display stack-up. Its frequency can range from several tens to hundreds of kHz. In the subsequent section, we will mainly focus on discussing how to suppress display noise, which has become increasingly influential due to the diminishing distance between the display pixel circuit and TSP electrodes in thin Active-Matrix Organic Light Emitting Diode (AMOLED) panel. The SMPS noise is induced by components such as mobile device chargers that come with power supplies and 3-phase lights. Therefore, a variety of methods to eliminate these diverse external noises are currently under investigation, one such approach being Code division multiple sensing (CDMS) [11].

During a display refresh time ($T_{refresh}$), a display drive IC (DDI) generates RGB update signals at every horizontal line update instant (T_{HSYNC}). As a result, a noise spike from the display update occurs periodically, which frequency is synchronized with the T_{HSYNC}. For instance, this repeats 1,920 times for a Full HD display, corresponding to the number of occurrences of the update signal, V_{DAC} [h]. These noises are ultimately coupled through the parasitic capacitor (C_{para_D}), which is formed between the display pixels and the cathode ground layer, which is also shared with the TSP readout

system. When the impedance of cathode ground is considerably larger than that of the TSP (C_{para_TSP}), the majority of display noises are transferred to the Rx electrode, as illustrated in Fig. 7.

The noise powers from the DAC driving of the DDI disseminate almost uniformly across all TSP regions. Each TSP Rx electrode (Rx[i+1], Rx[i+2], ... Rx[i+n]) experiences the same quantity of display noise. However, it is not the case that these noise signals are delivered to all channels with identical phase and amplitude. As depicted in Fig. 8, the noise injected into different channels via the display's cathode resistance ($R_{Cathode}$) experiences RC delay and voltage drop, leading to phase delay and gain attenuation. Consequently, compensation process must also be performed for noise that has experienced this phase delay and gain attenuation [12].

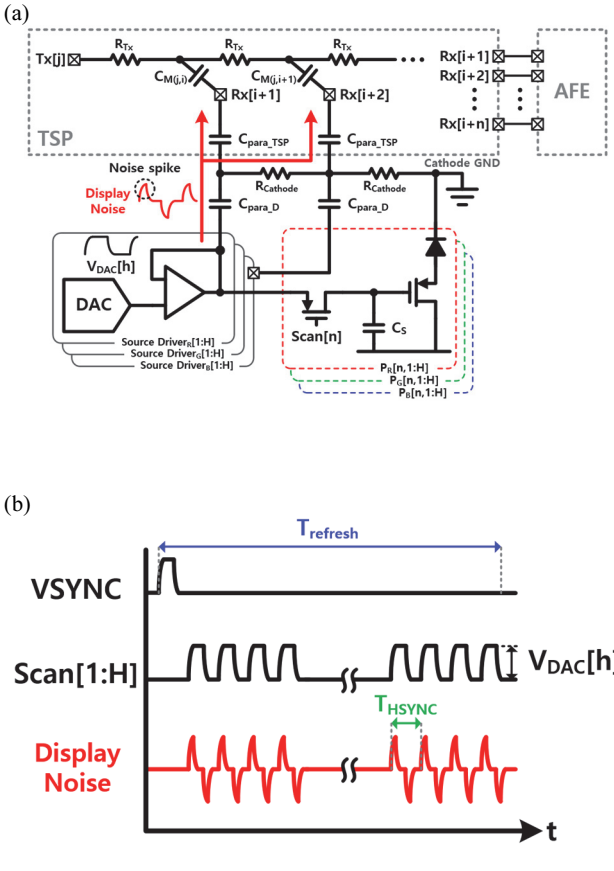

Fig. 7. (a) Equivalent circuit model of DDI, pixels and TSP and (b) display driving timing-diagram with display noise.

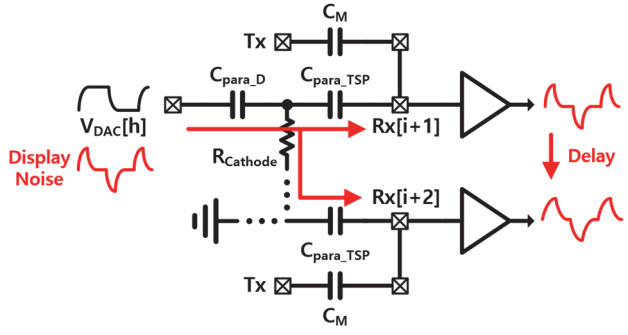

Fig. 8. Delay based on the RC value of the noise path.

3.3 Conventional solutions

3.3.1 Fully differential structure

Fully differential sensing operates based on the principle of using a differential pair of inputs to sense changes in touch capacitance. This method contrasts with single-ended sensing, which only uses a single input for sensing. By using a differential pair, this method can effectively cancel out common-mode noise, i.e., noise that appears equally on both inputs. Moreover, it can double the signal swing for the same supply voltage, enhancing the SNR [13-15]. The circuit in Fig. 9 is example of a fully differential architecture [16]. Those are designed to handle both C_S- and C_m-sensing modes. This architecture employs a differential charge amplifier (DCA) and an input common-mode control amplifier (CCA) to control the voltages of the two sensing lines.

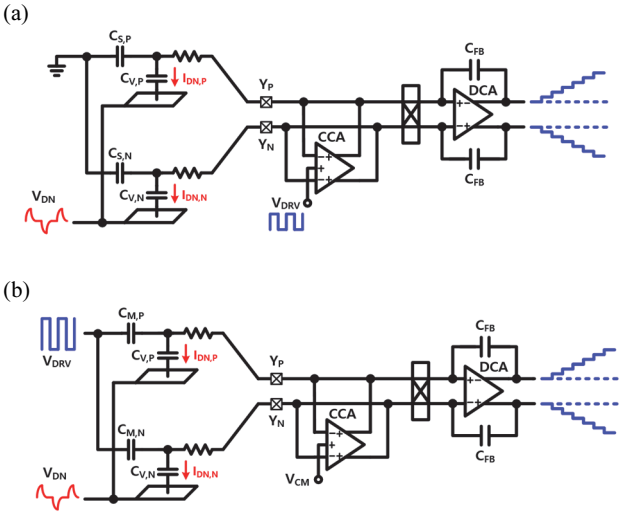

Fig. 9. Fully-differential sensing architecture (a) self-cap sensing method and (b) mutual-cap sensing method.

The CCA operates by balancing the voltages of these lines with a specific reference voltage, V_{DRV} and V_{CM}. This leads to the common-mode voltage of the sensing lines being equivalent to the reference voltage. Meanwhile, the DCA, assuming a sufficient open-loop gain and aided by negative feedback, works to minimize the input differential voltage while simultaneously converting charge to voltage.

In the C_S-sensing mode, the CCA's reference voltage is an ac voltage, V_{DRV}. The self-capacitors, $C_{S,P}$ and $C_{S,N}$, are driven by charging and discharging through V_{DRV}. Otherwise, In the C_S-sensing mode, the CCA's reference voltage is a DC voltage, V_{CM}, and Tx lines are stimulated by V_{DRV}. Assuming equal mutual capacitances, $C_{M,P}$ and $C_{M,N}$ between the neighboring sensor lines, equal currents flow through these lines, managed entirely by the CCA. If the display noise, V_{DN}, enters commonly through display parasitic capacitors, $C_{V,P}$ and $C_{V,N}$, the CCA effectively eliminates this noise component. This condition leads to a zero-differential output from the DCA. In contrast, if a touch event causes a disparity in the mutual capacitances, the DCA produces a differential voltage reflecting this difference.

The differential currents are alternated between the CCA and the DCA by the Multiplexer (MUX) switches in the current-mode demodulator (CDM). These switches operate on the same cycle as the transmitter Tx, alternately connecting two channels within a single cycle. These help to minimize the occurrence of offsets. This method prevents the aliasing problems commonly associated with discrete-time charge integrating techniques.

3.3.2 Chopper stabilization

ROICs often encounter 1/f noise and offset errors that can undermine their performance. Chopper stabilization, a technique originating in the analog domain, offers an effective solution for reducing these low-frequency errors, thus significantly enhancing the performance of touch sensor readout ICs.

As depicted in Fig. 10, The method works by modulating the signal at a frequency that is higher than the bandwidth of interest. The input signal, V_{IN}, initially gets modulated into a high-frequency signal (X), which subsequently mixes with a low-frequency noise signal, V_N, (Y). The mixed signal then undergoes amplification to increase its magnitude (Y'). Subsequently, demodulation takes place, during which the noise becomes high-frequency while the original signal reverts to low-frequency (Z). Lastly, a low-pass filter (LPF) is applied, suppressing the noise that has been shifted to high-frequency (Z'). The resultant signal is then demodulated back to its original form. The modulation and demodulation processes shift the low-frequency noise to the higher frequency band, thereby effectively minimizing its impact on the desired signal.

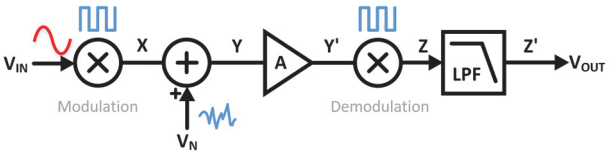

Fig. 10. Chopper amplification principle.

In the context of touch sensor readout ICs, chopper stabilization is utilized to minimize noise and offset errors. The technique is implemented at the amplifier stage of the readout ICs. By chopping the input signal, the DC offset and 1/f noise are pushed to higher frequencies, out of the bandwidth of interest. The resultant signal, now free from the detrimental effects of 1/f noise and offset errors, provides a more accurate touch detection, improving the overall performance of the touch sensor system.

Notably, it significantly reduces the 1/f noise and offset errors, improving the accuracy and reliability of the sensors. This results in better touch detection and an enhanced user experience.

3.3.3 Correlated double sampling

Analog correlated double sampling (CDS) is a method often used in sensor systems and image processors to reduce low frequency noise, offset, particularly the fixed-pattern noise.

The principle of operation of Analog CDS involves two main steps: First, a reference or 'reset' sample is taken. This sample, though it should theoretically represent a zero-level signal, can often contain various forms of noise, such as DC offset, thermal noise, or 1/f noise. After the reset sample, a signal sample is taken. This sample contains the desired signal but also includes the same noise that was present in the reset sample.

By taking the difference between the signal sample and the reset sample, Analog CDS effectively cancels out the noise

that is common to both, thereby providing a cleaner output signal. This is possible because the noise is 'correlated' between the two samples.

Despite several advantages, it is worth noting that Analog CDS is most effective at removing low-frequency noise; high-frequency noise may remain unattenuated.

4. NEWLY ADOPTED DESIGNS

In this section, we will delve into the exploration of diverse architectures currently under investigation, aimed at mitigating issues related to the significant self-capacitance previously discussed, and rectifying the display noise entering via substantial parasitic capacitance.

The demand for thin, flexible TSPs has grown recently due to the flexible nature of wearable devices. These thin panels merge with the display panel to form a single thin film. For instance, Samsung's Youm On-Cell Touch AMOLED (Y-OCTA) is an innovative display technology where the touch sensor is embedded directly into the display panel, unlike conventional touch screens that have a distinct layer for the touch sensor [17]. The benefit of this integrated approach is a thinner, lighter display which can potentially be produced at a lower cost. Furthermore, it may offer enhanced touch responsiveness, due to the decreased distance between the touch sensor and the elements of the display itself. However, one problem with the Y-OCTA display is that the touch electrode and display's cathode are too close, creating a large parasitic capacitance. Therefore, a circuit is needed to compensate for such large parasitic capacitance.

Several methods exist to compensate for large C_S [18]. One can provide compensation by using a capacitor of the same size to Sink & Source in the opposite phase. Another approach involves using a current to fill the exact charge that needs to be filled. Incorporating another large capacitor into the chip to compensate for a large capacitor is highly inefficient. Additionally, attaching a large capacitor to each channel runs counter to the current focus on lightweight and miniaturized mobile devices. Therefore, using a CC to compensate for multiple channel capacitors with a single capacitor is explained below. Furthermore, the size of that capacitor can be reduced by controlling the gain of the CC.

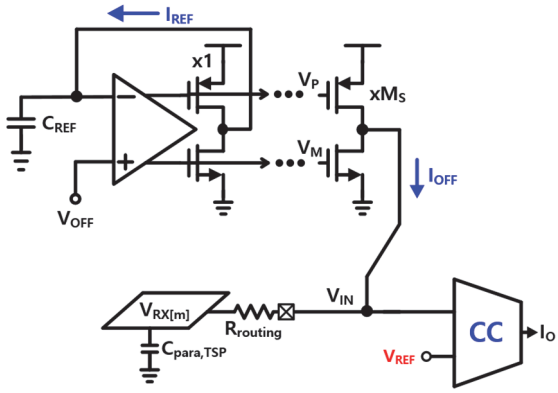

Fig. 11. Baseline compensator.

4.1 Baseline capacitance compensation

The compensation method to be discussed involves the use of large capacitors, which can lead to a problem known as 'slewing' when driven by limited current, particularly at high speeds. It fails to fully compensate for C_S. To address this issue, a circuit that allows additional current to flow when slewing occurs can be implemented, thereby enhancing the slew rate [19-21].

This structure was presented by Samsung LSI [22]. As depicted in Fig. 11, the baseline current compensator (BCC) is able to compensate for large capacitors by copying the charge that is being charged-discharged in C_{REF} due to V_{OFF} into a voltage form, and charging-discharging the desired amount of charge to parasitic capacitor, C_{para_TSP}. And the output transistors size of the BCC core is copied M_S by the Gain Controller and Gain-controlled transistors gate voltages, V_P and V_N, are transformed into a current form. This current, over a specific period of time, charges and discharges C_{para_TSP}, thereby creating the desired voltage. When the V_S node becomes the same voltage as V_{REF}, it indicates that the compensation has been fully achieved. Inherent to the CC's characteristics, if the two input nodes are identical, there will be no change in the output node.

If C_{REF} is 25 pF and C_P is 500 pF, a compensation of 20 times is required. Therefore, if the operating voltage size is V_{OFF}=V_{REF}, then M_S should be adjusted to 20 times. If the match is accurate and compensation is appropriately achieved and operating switch, Φ_{IN_EN}, is ON, there will be no current flowing through V_{OUT}.

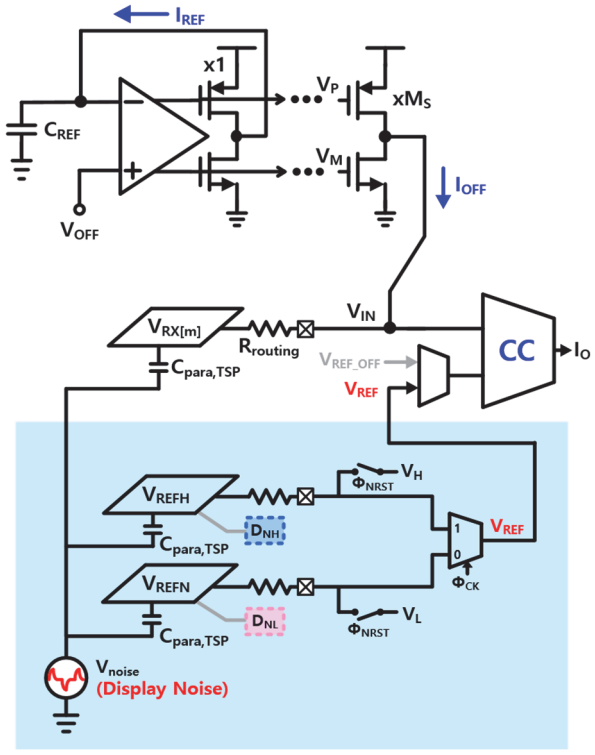

Fig. 12. Noise antenna reference scheme.

4.2 Improving noise immunity design

The design employs a baseline current compensator and a noise antenna reference scheme (NARS) to robustly counter the display noise injection. As depicted in Fig. 12, blue square, two additional channels are drawn out separately to serve as Reference channels besides the sensing TSP channel. The parasitic capacitor of TSP, $C_{para,TSP}$ of the two channels is primarily pre-charged to V_H and V_L respectively when Φ_{NRST} is closed, functioning as a voltage source. When NARS operates, the V_{IN} node and V_{REFN} are compared through CC, and current flows to I_O. If the BCC compensates accurately, there will be no current flowing to I_O.

However, if display noise exists, the same magnitude of noise is introduced to the sensing node and the reference node. This, in essence, swings the two CC input nodes to the same size, nullifying the effects of the noise. Nevertheless, as the capacitors of the reference and sensing channels are not entirely identical, and the sizes of the routing resistors do not match, a circuit compensating for these variations will also be necessary for precise noise elimination.

5. CONCLUSION

This review paper provides a comprehensive analysis of the principles, challenges, and recent advancements in the design of capacitive TSP ROICs. Capacitive TSPs are integral to a wide range of applications, particularly in the growing field of wearable devices. To meet the performance requirements, the readout systems must balance sensitivity and SNR while mitigating power consumption.

The paper first examined the fundamental operations of capacitive sensors and AFE circuits, highlighting the principles of C_S- and C_M-sensing methods. The readout circuits cater to these principles, converting sensed changes in capacitance into usable digital codes.

Next, we delved into the issue of noise, identifying internal and external noise sources and their detrimental effect on the system's SNR. Among the various types of noise, internally generated 1/f noise was recognized as a major concern. Various mitigation techniques were discussed, such as chopper stabilization and correlated double sampling, which effectively reduce low-frequency errors and improve overall system performance.

The paper then reviewed recent designs to compensate for the significant self-capacitance and to rectify display noise issues often encountered in on-cell structures like Samsung's Y-OCTA technology. The novel design that utilizes a BCC and NARS was described in detail, showcasing its ability to robustly counter display noise injection.

Touch sensor technology is rapidly advancing in the field of wearable technology, not only blurring the boundaries between humans and technology but also driving innovation in various fields. These flexible and stretchable touch sensors, capable of attaching to the complex structure of the body, can detect and quantify human interactions from simple touch to complex gestures. These sensors are expected to lead to breakthroughs in health monitoring, sports performance analysis, and intuitive human-computer interaction. Therefore, the future of touch sensors is anticipated to play a critical role in enriching human life through their integration with wearable technology.

Overall, the development of low-noise, high-performance TSP ROICs requires a thorough understanding of the sensing principles, coupled with an innovative approach to mitigating design and operational challenges. The methods and designs

discussed in this paper offer valuable insights for future advancements in this field, contributing to the evolution of wearable technology and beyond.

ORCID

Jong-Min Oh https://orcid.org/0000-0001-6303-2876
Seung-Hoon Ko https://orcid.org/0000-0001-6018-1104

ACKNOWLEDGEMENTS

This paper was supported by Korea Institute for Advancement of Technology (KIAT) grant funded by the Korea Government (MOTIE) (P0012451) and the National Research Foundation of Korea (NRF) grant funded by the Korea government (MSIT) (NRF-2021R1F1A1062391, NRF-2022R1F1A1074478).

REFERENCES

[1] A. H. Anwer, N. Khan, M. Z. Ansari, S. S. Baek, H. Yi, S. Kim, S. M. Noh, and C. Jeong, *Sensors*, **22**, 4460 (2022).
doi: https://doi.org/10.3390/s22124460

[2] Y. Huh, S. W. Hong, S. H. Park, C. Shin, J. S. Bang, C. Park, S. Park, and G. H. Cho, *IEEE J. Solid-State Circuits*, **53**, 1079 (2018).
doi: https://doi.org/10.1109/JSSC.2017.2772803

[3] S. H. Ko, *IEEE Sens. J.*, **20**, 4778 (2020).
doi: https://doi.org/10.1109/JSEN.2020.2966183

[4] S. H. Ko, *Proc. 2019 Symposium on VLSI Circuits* (IEEE, Kyoto, Japan, 2019) p. C218.
doi: https://doi.org/10.23919/VLSIC.2019.8778125

[5] Y. Hu, L. Huang, W. Rieutort-Louis, J. Sanz-Robinson, S. Wagner, J. C. Sturm, and N. Verma, 2*014 IEEE International Solid-State Circuits Conference Digest of Technical Papers (ISSCC)* (IEEE, San Francisco, USA, 2014) p. 212.
doi: https://doi.org/10.1109/ISSCC.2014.6757404

[6] T. G. Song, D. K. Kim, J. H. Cho. J. H. Lee, and H. S. Kim, *IEEE J. Solid-State Circuits*, **56**, 3470 (2021).
doi: https://doi.org/10.1109/JSSC.2021.3098732

[7] C. C. Enz and G. C. Temes, *Proc. IEEE*, **84**, 1584 (1996).
doi: https://doi.org/10.1109/5.542410

[8] H. Yoshizawa and G. C. *Temes, IEEE Trans. Circuits Syst. I*, **54**, 193 (2007).
doi: https://doi.org/10.1109/TCSI.2006.887454

[9] A. Bakker, K. Thiele, and J. H. Huijsing. *IEEE J. Solid-State Circuits*, **35**, 1877 (2000).
doi: https://doi.org/10.1109/4.890300

[10] J. S. An, S. J. Jung, S. K. Hong, and O. K. Kwon, *IEEE Sens. J.*, **17**, 803 (2016).
doi: https://doi.org/10.1109/JSEN.2016.2636137

[11] H. Shin, S. Ko, H. Jang, I. Yun, and K. Lee, *2013 IEEE International Solid-State Circuits Conference Digest of Technical Papers* (IEEE, San Francisco, USA, 2013).
doi: https://doi.org/10.1109/ISSCC.2013.6487782

[12] J. Lee, H. Kim, J. Ham, and S. Ko, *Micromachines*, **13**, 942 (2022).
doi: https://doi.org/10.3390/mi13060942

[13] S. H. Park, H. S. Kim, J. S. Bang, G. H. Cho, and G. H. Cho, *IEEE J. Solid-State Circuits*, **52**, 528 (2016).
doi: https://doi.org/10.1109/JSSC.2016.2621020

[14] I. S. Yang and O. K. Kwon, *IEEE Trans. Consum. Electron.*, **57**, 1027 (2011).
doi: https://doi.org/10.1109/TCE.2011.6018851

[15] M. Miyamoto, M. Hamaguchi, and A. Nagao, *IEEE J. Solid-State Circuits*, **50**, 335 (2015).
doi: https://doi.org/10.1109/JSSC.2014.2364092

[16] K. D. Kim, S. Kang, Y. K. Choi, K. H. Lee, C. H. Lee, J. C. Lee, M. Choi, K. Ko, J. Jung, N. Park, H. Park, and G. C. Hwang, *2014 Symposium on VLSI Circuits Digest of Technical Papers* (IEEE, Honolulu, USA, 2014) p. 1.
doi: https://doi.org/10.1109/VLSIC.2014.6858444

[17] Samsung Z Fold2 5G, Available online: https://www.samsung.com/us/smartphones/galaxy-z-fold2-5g/ (accessed on 1 June 2022).

[18] S. H. Ko and B. D. Yang, *IEEE Trans. Circuits Syst. II*, **66**, 1321 (2018).
doi: https://doi.org/10.1109/TCSII.2018.2888516

[19] M. G. Degrauwe, J. Rijmenants, E. A. Vittoz, and H. J. De Man, *IEEE J. Solid-State Circuits*, **17**, 522 (1982).
doi: https://doi.org/10.1109/JSSC.1982.1051769

[20] P. Pérez-Nicoli, F. Veirano, P. C. Lisboa, and F. Silveira, *2015 IEEE 6th Latin American Symposium on Circuits & Systems (LASCAS)* (IEEE, Montevideo, Uruguay, 2015) p. 1.
doi: https://doi.org/10.1109/LASCAS.2015.7250462

[21] B. Huang and D. Chen, *2014 IEEE 57th International Midwest Symposium on Circuits and Systems (MWSCAS)* (IEEE, College Station, USA, 2014) p. 270.
doi: https://doi.org/10.1109/MWSCAS.2014.6908404

[22] S. Byun, H. Lee, T. G. Song, J. Lee, J. Baek, G, Ha, S. Baek, Y. Kim, W. Jung, H. W. Lim, S. Kim, and J. Y. Lee, *2023 IEEE International Solid-State Circuits Conference (ISSCC)* (IEEE, San Francisco, USA, 2023) p. 386.
doi: https://doi.org/10.1109/ISSCC42615.2023.10067374